

7C02249



11340  
Olympic Blvd.  
Suite 355  
Los Angeles  
California  
90064-1639  
P (310) 268-0601  
F (310) 268-0701  
tdi@tdico.com

**BILL TO**

Ut-Battelle  
Bldg. 4500N, MS-6193  
PO Box 2008  
Oak Ridge, TN 37831-6193  
USA

**SHIP TO**

James Kidder  
Ut-Battelle

**Date Rec'd**

03/02/2007

**Need By**

**Ordered By**

P (865) 574-1241

F (865) 574-1240

**Requestor**

James Kidder

**Client Number**

52719X

**Service & Delivery**

REGULAR FedEx

**Journal/Book Title**

Chinese Science Bulletin

**Author 1**

Zhu WQ

**Author 2**

Pan YZ

Month	Year	Volume	Issue	Pages
	2006	51		457-63

**Article Title**

Simulation of maximum light use efficiency for some typical vegetation types in China

**Order Special Instructions**

MC: 4500N 6191

\*\*\*Further reproduction may be a violation of copyright law\*\*\*

## Simulation of maximum light use efficiency for some typical vegetation types in China

ZHU Wenquan<sup>1</sup>, PAN Yaozhong<sup>1</sup>, HE Hao<sup>1</sup>,  
YU Deyong<sup>1</sup> & HU Haibo<sup>2</sup>

1. Key Laboratory of Environmental Change and Natural Disaster of Ministry of Education, College of Resources Science and Technology, Beijing Normal University, Beijing 100875, China;

2. Institute of Urban Meteorology, China Meteorological Administration, Beijing 100089, China

Correspondence should be addressed to Pan Yaozhong (email: lunwen75@163.com)

**Abstract** Maximum light use efficiency ( $\epsilon_{\max}$ ) is a key parameter for the estimation of net primary productivity (NPP) derived from remote sensing data. There are still many divergences about its value for each vegetation type. The  $\epsilon_{\max}$  for some typical vegetation types in China is simulated using a modified least squares function based on NOAA/AVHRR remote sensing data and field-observed NPP data. The vegetation classification accuracy is introduced to the process. The sensitivity analysis of  $\epsilon_{\max}$  to vegetation classification accuracy is also conducted. The results show that the simulated values of  $\epsilon_{\max}$  are greater than the value used in CASA model, and less than the values simulated with BIOME-BGC model. This is consistent with some other studies. The relative error of  $\epsilon_{\max}$  resulting from classification accuracy is  $-5.5\% - 8.0\%$ . This indicates that the simulated values of  $\epsilon_{\max}$  are reliable and stable.

**Keywords:** light use efficiency, remote sensing, simulation, NPP, NDVI, China.

Maximum light use efficiency ( $\epsilon_{\max}$ ) is the use rate of photosynthetically active radiation by vegetation in an ideal condition without any constraints. It is a physiological attribute of plant itself. The value of  $\epsilon_{\max}$  is different for different vegetation types<sup>[1–5]</sup>. It is a key parameter for the estimation of net primary productivity (NPP) driven with remote sensing data. There are still many divergences about its value for each vegetation type<sup>[6]</sup>. Potter *et al.*<sup>[7]</sup> and Field *et al.*<sup>[8,9]</sup> took the global  $\epsilon_{\max}$  as  $0.389 \text{ gC}\cdot\text{MJ}^{-1}$ . Raymond<sup>[11]</sup> considered the upper limit of  $\epsilon_{\max}$  as  $3.5 \text{ gC}\cdot\text{MJ}^{-1}$ , and other studies indi-

cated that the  $\epsilon_{\max}$  of some herbaceous plants and other vegetations was  $0.09 - 2.16 \text{ gC}\cdot\text{MJ}^{-1}$  without constraints<sup>[2–5]</sup>. Peng *et al.*<sup>[6]</sup> took  $1.25 \text{ gC}\cdot\text{MJ}^{-1}$  as the  $\epsilon_{\max}$  to estimate the spatial distribution of light use efficiency in Guangdong Province of China. The result showed that the  $\epsilon_{\max}$  used in CASA model ( $0.389 \text{ gC}\cdot\text{MJ}^{-1}$ ) was lower when comparing to that of Guangdong vegetation. All of these studies indicated that the current values of  $\epsilon_{\max}$  for each vegetation type are not consistent, and a comprehensive analysis for  $\epsilon_{\max}$  should be conducted imperatively.

The  $\epsilon_{\max}$  acquired from field measurement can only represent the value in a little site, and it can not represent the  $\epsilon_{\max}$  of one kind of vegetation types<sup>[10]</sup>. The value of  $\epsilon_{\max}$  for each vegetation type is not only affected by its physiological attributes, but also the spatial scale and the uniformity of vegetation coverage. It can not be acquired by field measurement under the current study conditions, and it can only be simulated by models. Running *et al.*<sup>[11]</sup> simulated the  $\epsilon_{\max}$  of some typical vegetation types using an eco-physiological model BIOME-BGC. The sample data used in the simulation mainly came from North America. There are some regional differences when they are used in global or regional vegetation types.

In this paper, the  $\epsilon_{\max}$  for some typical vegetation types in China is simulated using a modified least squares function based on NOAA/AVHRR remote sensing data and field-observed NPP data. The vegetation classification accuracy is introduced to the process. The sensitivity analysis of  $\epsilon_{\max}$  to vegetation classification accuracy is also conducted.

### 1 Data acquisition and processing

#### 1.1 Remote sensing data

The NOAA/AVHRR (National Oceanic and Atmospheric Administration, Advanced Very High Resolution Radiometer) Normalized Difference Vegetation Index (NDVI) images came from the Pathfinder Data Set (PDS) which was sponsored by the Earth Resources Observation System (EROS). The spatial resolution is  $8 \text{ km} \times 8 \text{ km}$ . The monthly composite data were taken from January 1989 to December 1993. Atmosphere calibration was conducted, and cloud contamination was eliminated. The sensor degradation was revised with the assumption that the NDVI in deserts was zero. These images were rectified against the reference to-



will be affected by temperature and water. The  $\varepsilon$  for each grid is the product of the  $\varepsilon_{\max}$  ( $\text{gC}\cdot\text{MJ}^{-1}$ ) and the scales representing the availability of water ( $W$ ) and the suitability of temperature ( $f_1, f_2$ )<sup>[7]</sup>

$$\varepsilon(x, t) = f_1(x, t) \times f_2(x, t) \times W(x, t) \times \varepsilon_{\max}. \quad (2)$$

The two temperature scalars in this function attempt to capture two aspects of the regulation of plant growth by temperature. The water scalar is calculated in a monthly time step as a function of the ratio of estimated evapotranspiration (EET) to potential evapotranspiration (PET). The specific functions of  $f_1, f_2$  and  $W$  can be found in ref. [16].

Formulae (1) and (2) can be combined to one expression

$$\begin{aligned} \text{NPP}(x, t) = & \text{APAR}(x, t) \times f_1(x, t) \\ & \times f_2(x, t) \times W(x, t) \times \varepsilon_{\max}. \end{aligned} \quad (3)$$

For any NPP observed site, the  $\varepsilon_{\max}$  can be computed when the field measured NPP, APAR,  $f_1, f_2$  and  $W$  are known. The computed  $\varepsilon_{\max}$  is then classified according to the vegetation types. At last, the  $\varepsilon_{\max}$  for each vegetation type can be simulated using a modified least squares function based on the minimum error principle.

For one vegetation type, the errors between observed NPP and simulated NPP can be expressed as a function

$$E(x) = \sum_{i=1}^j (m_i - n_i x)^2 \quad x \in [l, u], \quad (4)$$

where  $i$  is the samples of one vegetation type;  $j$  is the maximum samples;  $m$  represents the observed NPP;  $n$  is the products of APAR;  $f_1, f_2$  and  $W$ ,  $x$  is an unknown variable representing the maximum light use efficiency that needs to be simulated; and  $l$  and  $u$  are the computed lower and upper limits of maximum light use efficiency based on formula (3). Formula (4) can be expanded as

$$E(x) = \sum_{i=1}^j n_i^2 x^2 - 2 \sum_{i=1}^j m_i n_i x + \sum_{i=1}^j m_i^2 \quad x \in [l, u]. \quad (5)$$

Formula (5) is a quadratic equation. It must have a minimum value when  $x$  is in the close range  $[l, u]$ . The  $x$  is just the simulated  $\varepsilon_{\max}$  of one vegetation type when the equation has a minimum value.

## 2.2 Estimation of APAR

APAR is calculated at each monthly time step. It is the product of PAR and the fraction of photosynthetic-

cally active radiation (FPAR)<sup>[6]</sup>. PAR can be calculated as 1/2 the total solar surface radiation (SOL) ( $\text{MJ}\cdot\text{m}^{-2}$ ). APAR is represented by

$$\text{APAR}(x, t) = \text{SOL}(x, t) \times \text{FPAR}(x, t) \times 0.5. \quad (6)$$

The theoretical relation between FPAR and NDVI was near-linear in some studies<sup>[2,17-19]</sup>. Assuming linearity, the equation for FPAR and NDVI can be solved when two points are known. These two points are the maximum and minimum NDVI values for each vegetation type and the corresponding FPAR values. The relation between FPAR and NDVI is then given by

$$\begin{aligned} \text{FPAR}(x, t) = & \frac{(\text{NDVI}(x, t) - \text{NDVI}_{i, \min}) \times (\text{FPAR}_{\max} - \text{FPAR}_{\min})}{(\text{NDVI}_{i, \max} - \text{NDVI}_{i, \min})} \\ & + \text{FPAR}_{\min}, \end{aligned} \quad (7)$$

with

$$\text{FPAR}_{\max} = 0.950,$$

$$\text{FPAR}_{\min} = 0.001,$$

$\text{FPAR}_{\max}, \text{FPAR}_{\min}$ , independent of vegetation type.  $\text{NDVI}_{i, \max}$ , NDVI value corresponding to 95% of NDVI population  $i$ .  $\text{NDVI}_{i, \min}$ , NDVI value corresponding to 5% of NDVI population  $i$ .

The landcover-type dependent NDVI values for 95% and 5% different vegetation populations will be specifically computed in section 3.1.

Further studies indicated that FPAR is also linearly related to the simple ratio (SR) which can be expressed as a transformation of NDVI (formula (9))<sup>[8,20,21]</sup>. The relation between FPAR and SR can be given by

$$\begin{aligned} \text{FPAR}(x, t) = & \frac{(\text{SR}(x, t) - \text{SR}_{i, \min}) \times (\text{FPAR}_{\max} - \text{FPAR}_{\min})}{(\text{SR}_{i, \max} - \text{SR}_{i, \min})} \\ & + \text{FPAR}_{\min}, \end{aligned} \quad (8)$$

where  $\text{SR}_{i, \max}$  and  $\text{SR}_{i, \min}$  are respectively corresponding to the  $\text{NDVI}_{i, \max}$  and  $\text{NDVI}_{i, \min}$ .

$$\text{SR}(x, t) = \left[ \frac{1 + \text{NDVI}(x, t)}{1 - \text{NDVI}(x, t)} \right]. \quad (9)$$

To see if one model is to be preferred over the other, FPAR was estimated with both models using the same minimum and maximum NDVI values. Comparison indicated a large bias in the estimate of FPAR from NDVI, a smaller bias in the estimate of FPAR from SR, and the smallest bias in the estimate of FPAR from the mean FPAR estimated by the SR-FPAR and NDVI-FPAR models<sup>[1]</sup>. The intermediate model is given by

1) Los, S. O., Linkages between global vegetation and climate: An analysis based on NOAA advanced very high resolution radiometer data, Ph. D. dissertation, National Aeronautics and Space Administration (NASA), 1998.

# ARTICLES

$$FPAR(x,t) = \alpha FPAR_{NDVI} + (1-\alpha) FPAR_{SR}, \quad (10)$$

with  $\alpha$  arbitrarily being set to 0.5.  $FPAR_{NDVI}$  is FPAR estimated with the NDVI-FPAR model (formula (7)) and  $FPAR_{SR}$  FPAR estimated with the SR-FPAR model (formula (8)). Given a situation without a priori information from which to choose the NDVI-FPAR or the SR-FPAR model, the intermediate model may be an alternative.

## 3 Results and discussion

### 3.1 Computation of the maximum NDVI value

The  $NDVI_{max}$  of one vegetation population is defined as the NDVI threshold that vegetation just came to fully green conditions, and it is not the actual maximum NDVI value in order to avoid the saturation phenomenon existing in NDVI. The vegetation classification accuracy was introduced to the computation of  $NDVI_{max}$ . It will be adjusted with the variation of classification accuracy. This may eliminate the errors existing in the classification and remote sensing data.

The processing chain of the  $NDVI_{max}$  computation contains the following three steps (Fig. 2): (1) The NDVI normalized frequency distributions were calculated for each of the vegetation types with equal inter-

vals of 0.0001 (Fig. 3). (2) According to the classification accuracy  $x$ , the pixels in the distribution range  $[(1-x)/2, (1+x)/2]$  are selected for each of the vegetation types. (3) These selected pixels are then calculated again to a normalized frequency distribution. The 95 percentile of the distribution for tall vegetation types and agriculture is assumed to represent vegetation at full cover and maximum activity with an FPAR value close to 1 (here assumed to be 0.95). The 95% NDVI value of agriculture was used to represent all short vegetation types. The 5% desert value is assumed to represent no vegetation and an FPAR value of 0.001 for all landcover types (Table 1).

### 3.2 Maximum light use efficiency of typical vegetation types in China

The maximum light use efficiency of some typical vegetation types in China is listed in Table 2. Bush and grassland had little measured data in this study. Their  $\epsilon_{max}$  was calculated with some data from references. The mean observed NPP of bush was  $364 \text{ gC}\cdot\text{m}^{-2}\cdot\text{a}^{-1[22-25]}$ . Its mean product  $n$  of APAR,  $f_1$ ,  $f_2$  and  $W$  was  $847.6 \text{ MJ}\cdot\text{m}^{-2}\cdot\text{a}^{-1}$ . So the  $\epsilon_{max}$  of bush was computed as  $0.429 \text{ gC}\cdot\text{MJ}^{-1}$ . The observed NPP of temperate grassland was  $230.6 \pm 64.9 \text{ gC}\cdot\text{m}^{-2}\cdot\text{a}^{-1[26]}$ . Its mean

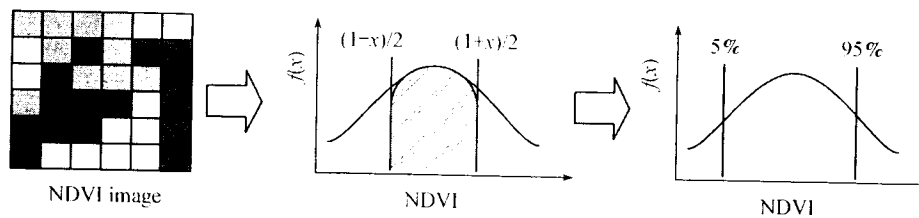


Fig. 2. Computation of  $NDVI_{max}$  and  $NDVI_{min}$ .

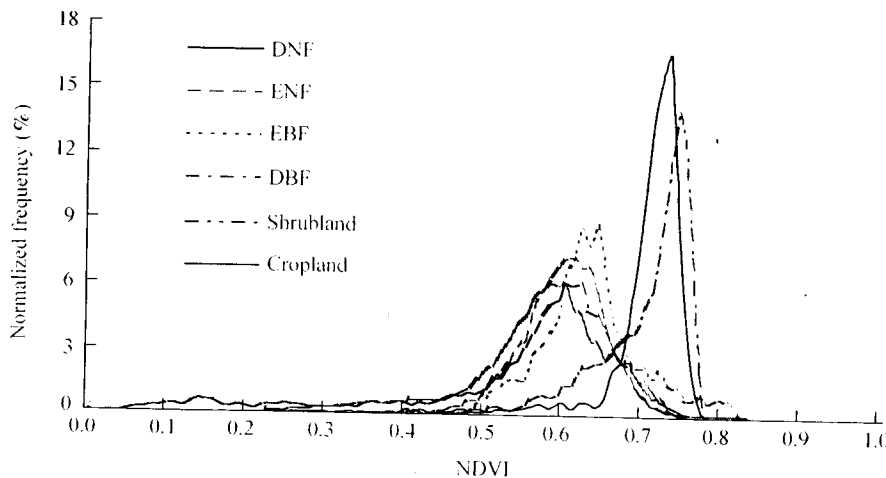


Fig. 3. The normalized frequency distribution of some vegetation types in China. DNF, Deciduous needle-leaf forest; ENF, evergreen needle-leaf forest; EBF, evergreen broadleaf forest; DBF, deciduous broadleaf forest; Shrubland, shrub vegetation; Cropland, agriculture vegetation.

Table 1 NDVI<sub>max</sub> and NDVI<sub>min</sub> of typical vegetation types in China

Code	Vegetation type	Pixels	NDVI <sub>max</sub>	NDVI <sub>min</sub>	SR <sub>max</sub>	SR <sub>min</sub>
1	deciduous needle-leaf forest	4339	0.738	0.023	6.63	1.05
2	evergreen needle-leaf forest	15104	0.647	0.023	4.67	1.05
3	evergreen broadleaf forest	6502	0.676	0.023	5.17	1.05
4	deciduous broadleaf forest	8690	0.747	0.023	6.91	1.05
5	bush	11905	0.636	0.023	4.49	1.05
6	sparse woods	958	0.636	0.023	4.49	1.05
7	seaside wet lands	287	0.634	0.023	4.46	1.05
8	alpine and sub-alpine meadow	11675	0.634	0.023	4.46	1.05
9	slope grassland	4364	0.634	0.023	4.46	1.05
10	plain grassland	7940	0.634	0.023	4.46	1.05
11	desert grassland	10184	0.634	0.023	4.46	1.05
12	meadow	11773	0.634	0.023	4.46	1.05
13	city	65	0.634	0.023	4.46	1.05
14	river	958	0.634	0.023	4.46	1.05
15	lake	1240	0.634	0.023	4.46	1.05
16	swamp	1015	0.634	0.023	4.46	1.05
17	glacier	1887	0.634	0.023	4.46	1.05
18	bare rocks	4528	0.634	0.023	4.46	1.05
19	gravels	13657	0.634	0.023	4.46	1.05
20	desert	12661	0.634	0.023	4.46	1.05
21	farmland	30046	0.634	0.023	4.46	1.05
22	alpine and sub-alpine plain grassland	10931	0.634	0.023	4.46	1.05

Table 2 Maximum light use efficiency of some typical vegetation types in China

Code	Vegetation type	Samples	$\epsilon_{\max}$ (gC·MJ <sup>-1</sup> )			Observed NPP (gC·m <sup>-2</sup> ·a <sup>-1</sup> )	Standard error of observed NPP	Range of observed NPP (gC·m <sup>-2</sup> ·a <sup>-1</sup> )	Simulated value from ref. [11] (gC·MJ <sup>-1</sup> )
			min.	max.	simulated value				
1	deciduous needle-leaf forest	39	0.159	2.453	0.485	490	160.9	179—824	1.103
2	evergreen needle-leaf forest	110	0.204	2.553	0.389	396	121.2	179—806	1.008
3	deciduous broadleaf forest	356	0.256	2.521	0.692	672	271.9	114—1669	1.044
4	evergreen broadleaf forest	142	0.407	2.194	0.985	1017	278.9	407—1913	1.259
5	mixed forest of needle and broad leaf	21	0.242	0.74	0.475	472	128.3	257—717	
6	mixed forest of evergreen and deciduous broadleaf	22	0.461	1.295	0.768	723	141.4	414—1098	1.116
7	bush	9			0.429	364			0.768
8	grassland				0.542	231	64.9		0.608
9	agriculture				0.542				0.604
10	others				0.542				

product  $n$  of APAR,  $f_1$ ,  $f_2$  and  $W$  was 425.6 MJ·m<sup>-2</sup>·a<sup>-1</sup>. So the  $\epsilon_{\max}$  of temperate grassland was computed as 0.429 gC·MJ<sup>-1</sup>. Other short vegetation types, such as agriculture, meadow, and swamp, have the same  $\epsilon_{\max}$  as grassland.

The simulated  $\epsilon_{\max}$  in this study is between the value used in the CASA model (0.389 gC·MJ<sup>-1</sup>) and the simulated value of BIOME-BGC model<sup>[11]</sup> except the evergreen needle-leaf forest, which is just equal to 0.389 gC·MJ<sup>-1</sup>. This is consistent with the study results of Peng *et al.*<sup>[6]</sup>, who concluded that the  $\epsilon_{\max}$  used in CASA model was lower when comparing to Guangdong vegetation. The simulated  $\epsilon_{\max}$  of BIOME-BGC, an eco-physiological processing model, is actually

based on plot-scale with little area. Its spatial scale is smaller and the vegetation has less heterogeneity in a little area. However, the simulation based on remote sensing data has a large spatial scale (8 km × 8 km in this study) and the heterogeneity is very high. So the simulated results should be lower than those of BIOME-BGC. The lower and upper limits of  $\epsilon_{\max}$  are also closer to some other study results<sup>[11-51]</sup>. This indicated that the simulated values in this study are reliable.

### 3.3 Sensitivity analysis of $\epsilon_{\max}$ to classification accuracy

The simulation of the  $\epsilon_{\max}$  was not only directly related to the vegetation types, but also indirectly related

# ARTICLES

to the classification accuracy. In order to simulate the  $\epsilon_{\max}$ , the FPAR value needs to be computed firstly, and it was related to the  $\text{NDVI}_{\max}$  and  $\text{SR}_{\max}$ . They are all calculated based on the vegetation type and the classification accuracy.

The classification accuracy was evaluated based on the field-observed data. There are some uncertainties in the evaluation. (1) The samples of observed data are relative less, and they are also not randomly distributed because of some artificial factors. Some place is difficult to arrive at, and there may be little samples there. (2) The spatial scale is not consistent between observed data and remote sensing data. The spatial heterogeneity will increase with the scale up. Several vegetation types may simultaneously exist in a large area. (3) There are some mixed types in the vegetation classification based on remote sensing data because of the approximate reflectance spectrums.

The landcover classification accuracy is 61.8% in this study. So the actual accuracy is assumed to be 35%–85% for each vegetation type, and then the 5% intervals are used to analyze the sensitivity of the  $\epsilon_{\max}$  to the classification accuracy.

The sensitivity analysis results are shown in Table 3 and Fig. 4. The  $\epsilon_{\max}$  increases with the increment of the accuracy for each vegetation type. The increasing trends can be classified to three types according to the sensitivity differences (Fig. 4). (1) The  $\epsilon_{\max}$  of evergreen broadleaf forest is very sensitive to the accuracy. Its absolute change is  $-0.054-0.079 \text{ gC}\cdot\text{MJ}^{-1}$ , and the relative change is  $-5.5\%-8.0\%$ . The change speed is very fast (Fig. 4(b)). (2) The sensitivity of deciduous broadleaf forest, mixed forest of evergreen and de-

ciduous broadleaf, grassland and other short vegetations is middle. The absolute change of  $\epsilon_{\max}$  is about  $-0.029-0.039 \text{ gC}\cdot\text{MJ}^{-1}$ , and the relative change is about  $-4.2\%-5.6\%$ . (3) The  $\epsilon_{\max}$  of deciduous needle-leaf forest, mixed forest of needle and broad leaf, evergreen needle-leaf forest and bush has a smallest sensitivity to classification accuracy. The smallest absolute change is  $-0.013-0.016 \text{ gC}\cdot\text{MJ}^{-1}$ , and the corresponding relative change is  $-2.7\%-3.3\%$ . Their change speeds are very slow. The curves fluctuate in a nearly horizontal line (Fig. 4 (b)). These sensitivity differences of the  $\epsilon_{\max}$  to the classification accuracy mainly come from the inner heterogeneity of each vegetation type and its classification accuracy. Taking evergreen broadleaf forest as an example, it has a highest sensitivity. Its classification accuracy is relatively low because of some mixed types, such as high bushes. On the other hand, it has a large heterogeneity because of many different sub-types and its extensive distribution in the whole country.

In general, the effect of the classification accuracy on the  $\epsilon_{\max}$  simulation is little, and the maximal relative error is just  $-5.5\%-8.0\%$ , which was found in the evergreen broadleaf forest. This indicated that the simulated  $\epsilon_{\max}$  for some typical vegetation types in China is reliable and stable. Though the true value of the  $\epsilon_{\max}$  can not be rigorously simulated, the approximate value can be given (Table 3). For example, the  $\epsilon_{\max}$  of deciduous needle-leaf forest is  $0.472-0.501 \text{ gC}\cdot\text{MJ}^{-1}$ , and the evergreen broadleaf forest  $0.931-1.064 \text{ gC}\cdot\text{MJ}^{-1}$ .

Table 3 The  $\epsilon_{\max}$  under different classification accuracy

Code <sup>a)</sup>	The $\epsilon_{\max}$ under different classification accuracy ( $\text{gC}\cdot\text{MJ}^{-1}$ )											
	61.8%	35%	40%	45%	50%	55%	60%	65%	70%	75%	80%	85%
1	0.485	0.472	0.473	0.475	0.476	0.478	0.481	0.483	0.486	0.49	0.496	0.501
2	0.389	0.374	0.377	0.378	0.381	0.384	0.387	0.391	0.395	0.40	0.406	0.412
3	0.692	0.663	0.667	0.672	0.676	0.682	0.688	0.695	0.702	0.71	0.721	0.731
4	0.985	0.931	0.939	0.948	0.956	0.966	0.979	0.992	1.006	1.023	1.043	1.064
5	0.475	0.462	0.464	0.464	0.466	0.468	0.471	0.474	0.477	0.48	0.484	0.488
6	0.768	0.732	0.737	0.743	0.748	0.756	0.765	0.774	0.784	0.794	0.808	0.821
7	0.429	0.408	0.412	0.415	0.418	0.422	0.427	0.431	0.436	0.442	0.448	0.454
8	0.542	0.509	0.513	0.519	0.524	0.532	0.538	0.549	0.556	0.565	0.577	0.589
9	0.542	0.509	0.513	0.519	0.524	0.532	0.538	0.549	0.556	0.565	0.577	0.589
10	0.542	0.509	0.513	0.519	0.524	0.532	0.538	0.549	0.556	0.565	0.577	0.589

a) The vegetation code is the same as in Table 2.

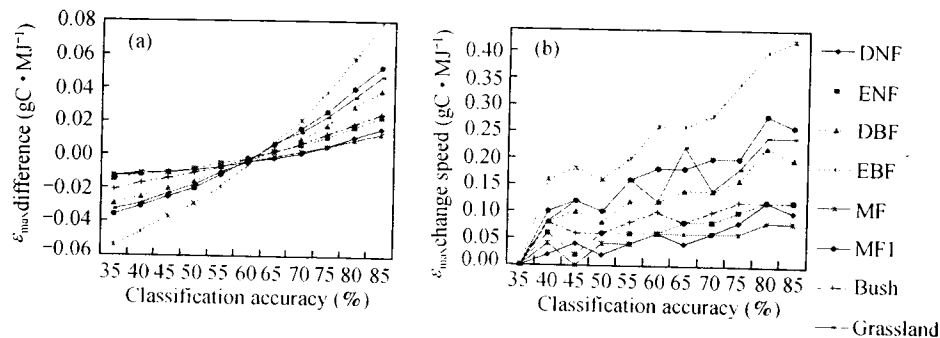


Fig. 4. The distribution of the  $\epsilon_{\max}$  change under different classification accuracy. (a) The difference between the simulated  $\epsilon_{\max}$  under different classification accuracy and that under 61.8%; (b) the  $\epsilon_{\max}$  change speed. DNF, Deciduous needle-leaf forest; ENF, evergreen needle-leaf forest; DBF, deciduous broadleaf forest; EBF, evergreen broadleaf forest; MF, mixed forest of needle and broad leaf; MF1, mixed forest of evergreen and deciduous broadleaf; Bush, shrub vegetation; Grassland, grassland vegetation.

**Acknowledgements** This work was supported by the National Natural Science Foundation of China (Grant No. 40371001) and the National Key Basic Research Program (Grant No. G2000018604).

## References

- Raymond, E., Hunt, J. R., Relationship between woody biomass and PAR conversion efficiency for estimating net primary production from NDVI, *International Journal of Remote Sensing*, 1994, 15: 1725–1730.
- Ruimy, A., Saugier, B., Methodology for the estimation of terrestrial net primary production from remotely sensed data, *Journal of Geophysical Research*, 1994, 97: 18515–18521.
- Goetz, S. J., Prince, S. D., Remote sensing of net primary production boreal forest stands, *Agricultural and Forest Meteorology*, 1996, 78: 149–179.
- Paruelo, J. M., Epstei, H. E., Lauenroth, W. K. *et al.*, ANPP estimates from NDVI for the central grassland region of the United States, *Ecology*, 1997, 78(3): 953–958.
- McCrary, R. L., Jokela, E. J., Canopy dynamics, light interception, and radiation use efficiency of selected loblolly pine families, *Forest Science*, 1998, 44(1): 64–72.
- Peng, S. L., Guo, Z. H., Wang, B. S., Use of GIS and RS to estimate the light utilization efficiency of the vegetation in Guangdong, China, *Acta Ecologica Sinica* (in Chinese), 2000, 20(6): 903–909.
- Potter, C. S., Randerson, J. T., Field, C. B. *et al.*, Terrestrial ecosystem production: a process model based on global satellite and surface data, *Global Biogeochemical Cycle*, 1993, 7: 811–841.
- Field, C. B., Randerson, J. T., Malmström, C. M., Global net primary production: Combining ecology and remote sensing, *Remote Sensing of Environment*, 1995, 51: 74–88.
- Field, C. B., Behrenfeld, M. J., Randerson, J. T. *et al.*, Primary production of the biosphere: integrating terrestrial and oceanic components, *Science*, 1998, 281: 237–240.
- Piao, S. L., Fang, J. Y., Guo, Q. H., Application of CASA model to the estimation of Chinese terrestrial net primary productivity, *Acta Phytocologica Sinica* (in Chinese), 2001, 25(5): 603–608.
- Running, S. W., Thornton, P. E., Nemani, R. *et al.*, Global terrestrial gross and net primary productivity from the earth observing system, in *Methods in ecosystem science* (eds. Sala, O., Jackson, R., Mooney, H.), New York: Springer Verlag, 2000, 44–57.
- Pan, Y. Z., Gong, D. Y., Deng, L. *et al.*, Smart distance Searching-based and DEM-informed interpolation of surface air temperature of climatology in China, *Acta Geographica Sinica* (in Chinese), 2004, 59(3): 366–374.
- Ni, J., Zhang, X. S., Scurlock, J. M. O., NPP Multi-Biome: Chinese Forests Data, 1989–1994, Available on-line [http://www.daac.ornl.gov/] from Oak Ridge National Laboratory Distributed Active Archive Center, Oak Ridge, Tennessee, U.S.A., 2001.
- Raich, J. W., Rastetter, E. B., Mellillo, J. M. *et al.*, Potential net primary productivity in South America: Application of a global model, *Ecological Applications*, 1991, 1: 399–429.
- Scurlock, J. M. O., Cramer, W., Olson, R. J. *et al.*, Terrestrial NPP: Towards a consistent data set for global model evaluation, *Ecological Applications*, 1999, 9(3): 913–919.
- Zhu, W. Q., Chen, Y. H., Pan, Y. Z. *et al.*, Estimation of light utilization efficiency of vegetation in China based on GIS and RS, *Geomatics and Information Science of Wuhan University* (in Chinese), 2004, 29 (8): 694–698.
- Hatfield, J. L., Asrar, G., Kanemasu, E. T., Intercepted photosynthetically active radiation in wheat canopies estimated by spectral reflectance, *Remote Sensing of Environment*, 1984, 14: 65–75.
- Sellers, P. J., Canopy reflectance, photosynthesis, and transpiration, *International Journal of Remote Sensing*, 1985, 6: 1335–1371.
- Huemrich, K. F., Goward, S. N., Spectral vegetation indices and the remote sensing of biophysical parameters, in *Proceeding of International Geoscience and Remote Sensing Symposium (IGARSS)*, Institute of Electrical and Electronics Engineers, Houston, Texas, 1992, 1017–1019.
- Los, S. O., Justice, C. O., Tucker, C. J., A global 1° by 1° NDVI dataset for climate studies derived from the GIMMS continental NDVI data, *International Journal of Remote Sensing*, 1994, 15: 3493–3518.
- Sellers, P. J., Randall, D. A., Collatz, J. A. *et al.*, A revised land-surface parameterization (SiB2) for GCMs, Part 1: Model Formulation, *Journal of Climate*, 1996, 9: 676–705.
- Jin, X. H., Liu, H. G., Song, Y. C., Study on the productivity of shrubbery in Yi County, Southern Anhui Province, *Acta Phytocologica et Geobotanica Sinica* (in Chinese), 1990, 14(3): 267–273.
- Chen, X. L., Ma, Q. Y., Kang, F. F. *et al.*, Studies on the biomass and productivity of typical shrubs in Taiyue Mountain, Shanxi Province, *Forest Research* (in Chinese), 2002, 15(3): 304–309.
- Tang, J. W., Zhang J. H., Song, Q. S. *et al.*, Biomass and net primary productivity of artificial tropical rainforest in Xishuangbanna, *Chinese Journal of Applied Ecology* (in Chinese), 2003, 14(1): 1–6.
- Liu, J. H., Xu X. X., Yang, G. *et al.*, Study on biomass of secondary shrubbery community in small watershed of Loess Hill and Gully Region, *Acta Botanica Borealis Occident Sinica* (in Chinese), 2003, 23(8): 1362–1366.
- Fan, J. W., Zhong, H. P., Liang, B. *et al.*, Carbon stock in grassland ecosystem and its affecting factors, *Grassland of China* (in Chinese), 2003, 25(6): 51–58.

(Received September 15, 2005; accepted October 11, 2005)